Real-space local self-motion of protonated and deuterated water

Yuya Shinohara,[1,*] Takuya Iwashita,[2] Masahiro Nakanishi,[3] Wojciech Dmowski,[4] Chae Woo Ryu,[4,†] Douglas L. Abernathy,[5] Daisuke Ishikawa,[6,7] Alfred Q. R. Baron,[6,7] and Takeshi Egami[1,4,8]

[1]*Materials Science and Technology Division, Oak Ridge National Laboratory, Oak Ridge, Tennessee 37831, USA*
[2]*Department of Integrated Science and Technology, Oita University, Dannoharu, Oita 870–1192, Japan*
[3]*Fukuoka Institute of Technology, 3-30-1 Wajiro-higashi, Higashi-ku, Fukuoka 811-0295 Japan*
[4]*Department of Materials Science and Engineering, The University of Tennessee, Knoxville, Tennessee, 37996 USA*
[5]*Neutron Scattering Division, Oak Ridge National Laboratory, Oak Ridge, Tennessee 37831, USA*
[6]*Materials Dynamics Laboratory, RIKEN SPring-8 Center, Sayo, Hyogo 679–5148, Japan*
[7]*Japan Synchrotron Radiation Research Institute, Sayo, Hyogo 679–5198, Japan*
[8]*Department of Physics and Astronomy,The University of Tennessee, Knoxville, Tennessee, 37996 USA*

(Received 2 February 2024; accepted 17 May 2024; published 11 June 2024)

We report on the self-part of the Van Hove correlation function, the correlation function describing the dynamics of a single molecule, of water and deuterated water. The correlation function is determined by transforming inelastic scattering spectra of neutrons or x rays over a wide range of momentum transfer Q and energy transfer E to space R and time t. The short-range diffusivity is estimated from the Van Hove correlation function in the framework of the Gaussian approximation. The diffusivity has been found to be different from the long-range macroscopic diffusivity, providing information about local atomic dynamics.

DOI: 10.1103/PhysRevE.109.064608

I. INTRODUCTION

Understanding the transport properties of water is of paramount importance. Despite the numerous studies, the description of its macroscopic transport properties based on microscopic knowledge is still under debate [1,2]. Self-motion of molecules is one of the fundamental properties that characterize liquid [3,4]. The self-diffusion coefficient has been determined using several experimental techniques. For example, tracer measurement and pulsed magnetic field gradient nuclear magnetic resonance (NMR) characterize a macroscopic diffusive motion where the hydrodynamic description is appropriate [5–10]. Quasielastic neutron scattering (QENS) characterizes a diffusive motion in liquid at the nanometer scale [3]; the width of the quasielastic line in the incoherent neutron scattering spectra is related to the translational and rotational diffusive motion, and its Q dependence is compared to diffusion models, where Q is the magnitude of scattering vector [11]. Using incoherent QENS, the self-motion of bulk liquid water has been studied [12–15].

In most cases, QENS measurements are carried out at a relatively low Q, typically $Q < 2\,\text{Å}^{-1}$, where the incoherent neutron scattering predominates over the coherent neutron scattering [11]. This reciprocal length scale corresponds to the correlation length of multiple collisions among the particles, making QENS using incoherent neutron scattering at low Q suitable for discussing diffusion behavior at the nanometer scale. In contrast, observation of quasielastic and inelastic scattering of x rays and neutrons at higher Q can provide information on dynamics before and at the onset of diffusive behavior, at which point the hydrodynamic description is not justified. However, separating self- and correlated motion in this Q range is not trivial in reciprocal space.

By converting the scattering spectra in reciprocal space into the correlation function in real space, we can separate the self- and correlated motion, particularly at the onset of diffusive motion [16]. Thanks to the development of high-resolution x-ray scattering [17,18] and time-of-flight inelastic neutron scattering [19], it is now feasible to measure the inelastic x-ray scattering (IXS) and inelastic neutron scattering (INS) over a wide range of energy transfer and momentum transfer with an energy resolution that is high enough to identify the atomic-scale dynamics within a reasonable amount of time. Measuring INS and IXS over a wide Q range that is usually ignored in the study of liquid enables us to convert the dynamic structure factor into the real-space spatiotemporal correlation function, the Van Hove correlation function (VHF), $G(R, t)$ [20]:

$$G(R,t) = \frac{1}{4\pi\rho NR^2}\sum_{i,j}\delta(R - |\boldsymbol{r}_i(0) - \boldsymbol{r}_j(t)|),$$

where ρ is the atomic number density, and $\boldsymbol{r}_j(t)$ is the position of the ith atom at time t. $\delta(r)$ is Dirac's delta function. The VHFs consist of two parts: the self-part, $G_s(R, t)$, and the distinct part, $G_d(R, t)$, such that

$$G_s(R,t) = \frac{1}{4\pi\rho NR^2}\sum_{j}\delta(R - |\boldsymbol{r}_j(0) - \boldsymbol{r}_j(t)|),$$

$$G_d(R,t) = \frac{1}{4\pi\rho NR^2}\sum_{i\neq j}\delta(R - |\boldsymbol{r}_i(0) - \boldsymbol{r}_j(t)|).$$

*Corresponding author: shinoharay@ornl.gov
†Present address: Department of Materials Science and Engineering, Hongik University, Seoul 04066, South Korea.

The self-part represents the probability of finding an atom j at distance R and time t, given that it is at $R = 0$ at $t = 0$. Thus, the self-part of the VHF describes the single-particle dynamics.

In this paper, we investigate the self-part of the VHF of H_2O and D_2O determined by INS and IXS at the subpicosecond timescale. Using x rays and neutrons allows us to look at the motion of different elements. Neutron scattering of H_2O is dominated by incoherent scattering from hydrogen, so the spectra mostly correspond to the self-motion of hydrogen. In contrast, x-ray scattering of H_2O is dominated by coherent scattering from oxygen, resulting in the dominant contribution being the self- and correlated motion of oxygen. The neutron scattering of D_2O is conventionally used to discuss the collective motion instead of the self-motion because the coherent neutron scattering cross section of deuterium is relatively high. Therefore, the self-motion of D_2O has been hardly measured using neutrons. The conversion into the real-space correlation function enables us to separate the self-motion in the same way as the x-ray scattering. In this work, we analyze the self-part of the VHF using the Gaussian approximation and discuss the local self-motion of H_2O and D_2O.

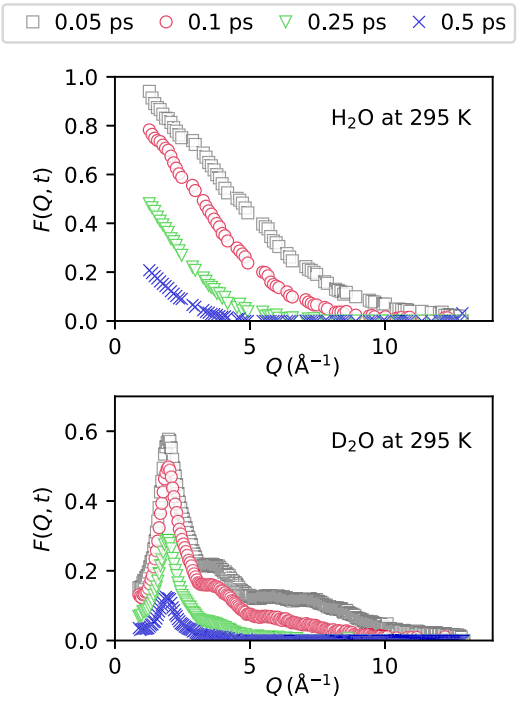

FIG. 1. Intermediate scattering function of (top) H_2O and (bottom) D_2O at 295 K determined by INS. For clarity, the profiles at $t = 0.05$, 0.1, 0.25, and 0.5 ps are shown. The gaps observed in the spectra for H_2O are due to the elimination of the Bragg peaks of aluminum used as the sample can.

II. METHODS

A. Inelastic neutron scattering

Inelastic neutron scattering experiment of H_2O and D_2O were carried out using the ARCS instrument [21] in the Spallation Neutron Source (SNS) at Oak Ridge National Laboratory (U.S.A.). As the energy of incident neutrons, 100 meV was chosen to cover a range of energy transfer E and momentum transfer Q that are wide enough to convert the dynamic structure factor $S(Q, E)$ into the VHF. A thin-walled annular double-walled container made of aluminum was used as a sample container for H_2O. This container is made of a hollow cylinder into which another hollow cylinder is fit. The annular thickness was chosen to be 0.1 mm to reduce the amount of multiple scattering due to a strong incoherent neutron scattering of hydrogen. The diameter of the container was 29 mm. Bragg peaks and phonon spectra of aluminum in inelastic scattering region overlap with the spectra of H_2O, but the contamination of the Bragg peaks can be avoided by choosing the Q points between them and the phonon contribution can practically be ignored due to the large incoherent scattering of hydrogen. A thin-walled annulus container made of vanadium was used as a sample container for D_2O. The annular thickness and the diameter of the vanadium container were 0.5 and 27 mm, respectively.

The sample container was placed in a closed-cycle refrigerator (CCR-16) to control the sample temperature at 285, 295, 310, 318, 334, and 343 K (343 K was only for H_2O). The radial collimator was inserted to reduce the background scattering from the CCR-16. The beam size at the sample position was 35 mm (H) and 35 mm (V). The spectra were reduced to the dynamic structure factor $S(Q, E)$ by using the MANTID suite [22], and then converted into the intermediate scattering function $F(Q, t)$ via Fourier transformation over E. The effect of instrument energy resolution was removed in the time domain by dividing the intermediate scattering functions by the Fourier transform of the instrument energy resolution function over energy transfer [23].

B. Inelastic x-ray scattering

High-resolution inelastic x-ray scattering experiments of H_2O at 334 and 343 K were carried out at BL43LXU, SPring-8 (Japan) [24] where world-leading intensity on the sample and the largest available, 24–28 element, analyzer array facilitated measurements over the required large range of energy and momentum transfer [17]. The results at 283, 295, 310, and 318 K are taken from our earlier work [16]. The details of experimental setting and data reduction procedure are described in previous papers [16,25]. The liquid sample was placed between two single-crystal diamond windows and the thickness of the sample was 1 mm. The spectra were measured over $-5\,\text{meV} < E < 70\,\text{meV}$ and $1\,\text{Å}^{-1} < Q < 10\,\text{Å}^{-1}$ with ~meV resolution.

III. RESULTS AND DISCUSSION

A. Obtaining the self-part of the Van Hove correlation function

Figure 1 shows the intermediate scattering function $F(Q, t)$ of H_2O and D_2O at 295 K determined by INS through the Fourier transformation of $S(Q, E)$ from E to t. The profiles of H_2O and D_2O are completely different: $F(Q, t)$ of H_2O decays monotonically and rapidly with Q, particularly at longer times, while $F(Q, t)$ of D_2O shows oscillation that is superimposed on the decaying behavior. This difference

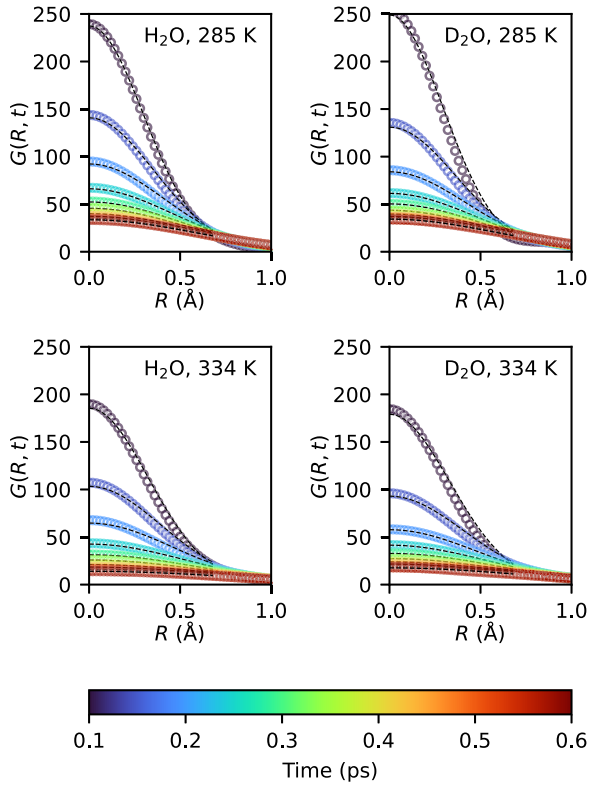

FIG. 2. The Van Hove correlation function of H_2O (left panels) and D_2O (right panels) around $R = 0$ at 285 K (top panels) and 334 K (bottom panels). The symbols represent the experimental data and the dashed lines represent the fitting results using the Gaussian approximation. The data are for $0.1 < t < 0.6$ ps. The interval between each time slice is 0.025 ps.

can be explained by the different scattering contrasts. The incoherent scattering of hydrogen atoms dominates the inelastic scattering from H_2O: the bound coherent and incoherent neutron scattering cross sections of hydrogen are 1.7583 and 80.27 barns, respectively. Because the incoherent scattering does not contain information about the correlation between atoms, $F(Q,t)$ of H_2O primarily represents the self-motion of hydrogen. In contrast, the inelastic scattering from D_2O cannot be attributed to the single element and is the sum of several contributions: the bound coherent and incoherent neutron scattering cross sections are 5.592 and 2.05 barns (deuterium) and 4.232 and 0.000 barns (oxygen), respectively [26]. Therefore, only the incoherent scattering from oxygen can be ignored, and $F(Q,t)$ of D_2O is composed of the self-part of deuterium and the distinct part representing the correlation between the atoms. This correlation part leads to the appearance of oscillation, as shown in the figure. This oscillation is similar to those observed in $F(Q,t)$ determined by IXS, where the oxygen-oxygen correlation was observed together with the self-part of oxygen [16]. This observation illustrates that the oscillating signals characterize the distinct part and the monotonic decrease along Q characterizes the self-part. It is, however, still not straightforward to separate these two different contributions.

The self-part and the distinct part were distinguished by calculating the VHF via the Fourier transformation of $F(Q,t)$ over Q. This conversion from reciprocal space to real space often adds unwanted oscillation due to the termination error associated with the finite Q range, as is well known in pair distribution function studies. As discussed and demonstrated in [16], the effect of termination errors can be mitigated because of the decaying behavior of the self-part of $F(Q,t)$ at a high-Q range. In particular, when the value of $F(Q_{\max},t)$ is nearly zero, where $Q_{\max}$ represents the maximum Q in the measurement, the finite Q range hardly affects the result of Fourier transformation. In the current case shown in Fig. 1, the value at $Q_{\max} = 12.9\,\text{Å}^{-1}$ has a finite value at $t = 0.05$ ps but is close to zero at $t = 0.1$ ps. Therefore, we can justify that the VHF can reliably be calculated at $t \geqslant 0.1$ ps for $T = 295$ K. We examined the effect of finite Q range for other temperatures and used only the data without the effect of termination errors in the following discussion.

The result of conversion into the VHF based on the INS results is shown in Fig. 2. The short-time limit, 0.1 ps, was set by the termination errors as discussed above. In contrast, the long-time limit, 0.6 ps, was set by the finite energy resolution of the instrument, 3–5 meV, in the current study. In this work, we focus on the self-part of the VHF at $R < 1.0$ Å in this time range, while the distinct part of the VHF, which is more prone to termination errors, will be discussed in future work. As the temperature increases, the height of the self-part at $R = 0$ decreases, indicating faster self-motion at higher temperatures. We discuss the self-motion based on the VHF in the next section.

B. Real-space self-motion of H_2O and D_2O

We first analyzed the VHF using the Gaussian approximation:

$$G_s(R,t) = \frac{1}{\rho}\left[\frac{1}{\pi\alpha(t)}\right]^{3/2}\exp\left(-\frac{R^2}{\alpha(t)}\right),$$

where $\alpha(t)$ characterizes the self-motion of particles: $\alpha(t) = 4Dt$ at the hydrodynamic limit and $\alpha(t) = 2k_BTt^2/m$ for the ideal gas [3,4]. Within the time range of the current study ($0.1 \leqslant t \leqslant 0.6$ ps), the Gaussian approximation reasonably fits the data, as shown in Fig. 2. Even though a small discrepancy from the Gaussian behavior is observed, the agreement is significant since there is only one parameter, $\alpha(t)$, to fit the curve. For $t > 0.6$ ps, uncertainty is large due to the finite energy resolution of instruments, so we do not include the longer time-scale behavior in our discussion.

Using the fitting results, we calculated the time evolution of the mean-squared displacement, $\langle r^2(t)\rangle = 3\alpha(t)/2$, as shown in Fig. 3. Both H_2O and D_2O show qualitatively similar behavior: (a) $\langle r^2(t)\rangle$ is larger at a higher temperature, (b) at $t < 0.3$ ps, $\langle r^2(t)\rangle$ mostly follows $\langle r^2(t)\rangle \sim t$ with a slope that is only weakly temperature dependent, and (c) at $t > 0.3$ ps, $\langle r^2(t)\rangle \sim t$ with a temperature-dependent slope. These behaviors are similar to those observed for $\langle r^2(t)\rangle$ of oxygen determined by the IXS measurement [16]. In the present study, we do not see the gaslike ballistic dynamics characterized by $\langle r^2(t)\rangle \sim t^2$ behavior, which is typically expected at a short timescale. The absence of gaslike behavior is likely because the minimum t (0.1 ps) in the present work

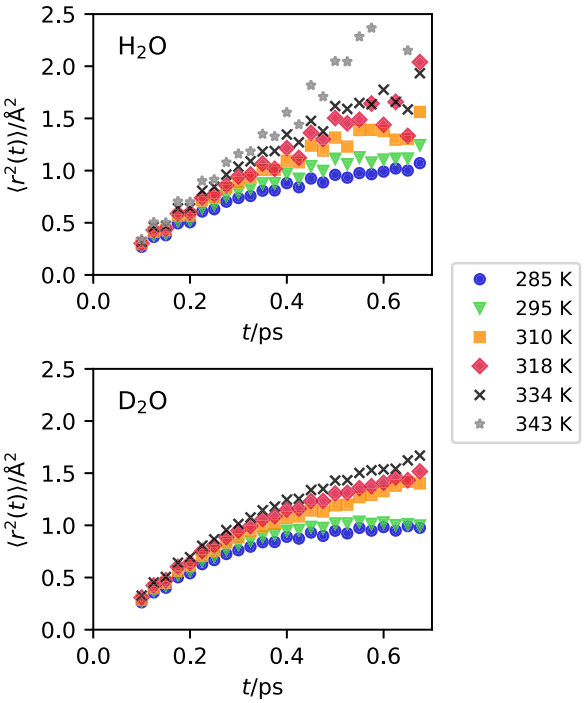

FIG. 3. Temporal evolution of the mean-squared displacement calculated using the Gaussian approximation for (top) H_2O and (bottom) D_2O based on the INS results.

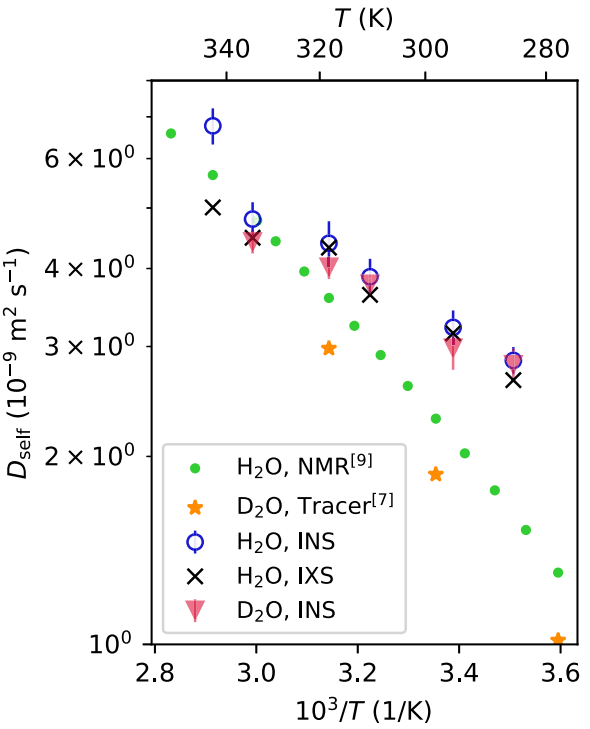

FIG. 4. Self-diffusion coefficient of H_2O and D_2O. Open circles: H_2O from the INS experiment; crosses: H_2O from the IXS experiment [16]; closed triangles: D_2O from the INS experiment; closed dots) H_2O from Ref. [10]; stars: D_2O from Ref. [7]. Uncertainty in the INS results was estimated by the standard deviation of the fitting.

is not short enough to access those dynamics, ~ 0.025 ps as suggested by a coherent x-ray scattering measurement [27].

To compare the results of INS and IXS, we estimated the average value of the short-time self-diffusion coefficient D_{VHF} by calculating the slope in Fig. 3, averaged over $0.5\,\mathrm{ps} < t < 0.65\,\mathrm{ps}$. The temperature dependence of D_{VHF} is shown in Fig. 4. First, compare the IXS and INS results of H_2O. D_{VHF} determined by INS is always larger than that by IXS in this temperature range, but the difference is small except for $T = 343\,\mathrm{K}$. The self-motion of H_2O observed by INS mostly represents the motion of hydrogen atoms due to the strong incoherent neutron scattering of hydrogen. In contrast, the self-motion of H_2O observed by IXS is governed by the self-motion of oxygen because the number of electrons of a hydrogen atom is much smaller than that of an oxygen atom. Hence, the motion of the hydrogen atom is almost invisible compared to that of the oxygen atom in IXS. The lack of large difference in D_{VHF} determined by IXS and INS despite their different scattering contrast indicates that the IXS and INS observe the motion of a whole molecule, which is supported by the fact that the self-ionization of water is very small. The remaining difference may be attributed to the rotational motion of the water molecule; the rotational motion might contribute to $\langle r^2(t)\rangle$ and D_{VHF} in the INS results, while it is less significant in the IXS results, where the oxygen motion is primarily measured. We cannot exclude the possibility that some systematic errors due to, e.g., the thermometer, are the source of this difference because the IXS and INS are separate measurements.

Now we compare the INS results of D_2O and H_2O. In this temperature range, the short-time self-diffusion coefficient D_{VHF} of D_2O is smaller than that of H_2O; $D_{\mathrm{VHF}}(H_2O)/D_{\mathrm{VHF}}(D_2O)$ are 1.02 (285 K), 1.08 (295 K), 1.03 (310 K), 1.09 (318 K), and 1.09 (334 K) in our current measurement. These values are comparable to the square root of the molecular mass ratio, $[m(D_2O)/m(H_2O)]^{1/2} = 1.05$, supporting classical theories that predict an inverse square root of mass dependence of the self-diffusion coefficient [8,28]. Meanwhile, this value is smaller than the ratio of macroscopic self-diffusion coefficients of H_2O and D_2O, which is 1.26 in a tracer experiment [7] and 1.27 in NMR measurements [29], and the ratio of viscosities, which is 1.23 [8]. These deviations of macroscopic self-diffusion data from the simple law have been partially explained in terms of the rotational moment of inertia [8]. Because our INS results are comparable to the prediction of the inverse square root of mass dependence, the rotational motion can likely be ignored in this timescale, which is also supported by the molecular dynamics simulation where the rotational jump times are estimated to be 2–3 ps in this temperature range [30]. This observation also supports the lack of large discrepancies in the values of D_{VHF} determined by IXS and INS despite their different scattering contrasts.

There is also a discrepancy between D_{VHF} determined in this work and a macroscopic self-diffusion coefficient D_{Macro}. This discrepancy is highlighted at lower temperatures. As discussed in [16], this discrepancy most likely originates from the differences between long- and short-range diffusivity. D_{Macro} is defined rather macroscopically for diffusion in the

hydrodynamic limit. Even the QENS measurement of self-diffusion measures the diffusive motion after multiple collisions. In contrast, the VHFs calculated from the INS and the IXS spectra measure the onset of the diffusion process at short time and length scales. Every molecule is mobile in liquids and participates in molecular transport, leading to strongly correlated molecular motions at an atomic scale. In contrast, the lattice structure will define the diffusional jump distance for an atom in crystalline systems. Such clear restriction does not exist in liquids. Further study of this local self-motion in other types of liquids, such as metallic and ionic liquids, using this real-space approach, will help identify the nature of dynamic correlations in liquids.

In the current work, the motion associated with the proton hopping was not distinguished, and the self-part of the VHF was analyzed using the Gaussian approximation. Further studies using acid solutions may disentangle the molecular motion from the motion associated with the proton hopping in this sub-ps time scale. For example, a recent two-dimensional infrared spectroscopy of proton transfer in water used a concentrated hydrochloric acid solution, and the proton hopping time was extrapolated to the dilute limit [31]. By choosing an acid with a low neutron scattering contrast and utilizing a high incoherent neutron scattering of hydrogen, it should be possible to carry out the INS measurement for water in a highly self-ionized environment.

IV. CONCLUSION

The self-part of the Van Hove correlation functions of H_2O and D_2O has been determined by experiments with inelastic neutron scattering and high-resolution inelastic x-ray scattering. Using the scattering spectra over the wide range of momentum and energy transfer, we avoided the difficulty in converting the scattering spectra in reciprocal space into the real-space correlation function. The results show that the short-time local self-dynamics of water molecules are different from the long-range diffusion at the hydrodynamic limit. The difference in short-time diffusion coefficients between H_2O and D_2O is close to the square root of the molecular mass ratio.

ACKNOWLEDGMENTS

Work by Y.S., W.D., C.W.R., and T.E. was supported by the U.S. Department of Energy (DOE), Office of Science, Office of Basic Energy Science, Materials Science and Engineering Division, under Contract No. DE-AC05-00OR22725. A portion of this research used resources at the Spallation Neutron Source, a DOE Office of Science User Facility operated by the Oak Ridge National Laboratory. The IXS experiments at BL43LXU, SPring-8, were carried out under the approval of RIKEN (Proposals No. 20170075, No. 20180069, and No. 20210019).

[1] P. Ball, Water—an enduring mystery, Nature (London) **452**, 291 (2008).

[2] K. Amann-Winkel, M.-C. Bellissent-Funel, L. E. Bove, T. Loerting, A. Nilsson, A. Paciaroni, D. Schlesinger, and L. Skinner, X-Ray and neutron scattering of water, Chem. Rev. **116**, 7570 (2016).

[3] J. P. Boon and S. Yip, *Molecular Hydrodynamics* (McGraw-Hill, New York, 1980).

[4] J.-P. Hansen and I. R. McDonald, *Theory of Simple Liquids*, 3rd ed. (Academic, London, 2006).

[5] J. H. Wang, Self-diffusion coefficients of water, J. Phys. Chem. **69**, 4412 (1965).

[6] K. T. Gillen, D. C. Douglass, and M. J. R. Hoch, Self-diffusion in liquid water to −31 °C, J. Chem. Phys. **57**, 5117 (1972).

[7] R. Mills, Self-diffusion in normal and heavy water in the range 1–45 deg, J. Phys. Chem. **77**, 685 (1973).

[8] H. Weingärtner, Self diffusion in liquid water. A reassessment, Z. Phys. Chem. **132**, 129 (1982).

[9] W. S. Price, H. Ide, and Y. Arata, Self-Diffusion of supercooled water to 238 K using PGSE NMR diffusion measurements, J. Phys. Chem. A **103**, 448 (1999).

[10] M. Holz, S. R. Heil, and A. Sacco, Temperature-dependent self-diffusion coefficients of water and six selected molecular liquids for calibration in accurate ^{1}H NMRPFG measurements, Phys. Chem. Chem. Phys. **2**, 4740 (2000).

[11] M. Bée, Quasielastic neutron scattering, principles and applications in solid state chemistry, *Biology and Materials Science* (Adam Hilger, Bristol, 1988).

[12] B. N. Brockhouse, Structural dynamics of water by neutron spectrometry, Nuovo Cim. **9**, 45 (1958).

[13] M. Sakamoto, B. N. Brockhouse, R. G. Johnson, and N. K. Pope, Neutron inelastic scattering study of water, J. Phys. Soc. Jpn. **17**, 370 (1962).

[14] J. Teixeira, M.-C. Bellissent-Funel, S. H. Chen, and A. J. Dianoux, Experimental determination of the nature of diffusive motions of water molecules at low temperatures, Phys. Rev. A **31**, 1913 (1985).

[15] J. Qvist, H. Schober, and B. Halle, Structural dynamics of supercooled water from quasielastic neutron scattering and molecular simulations, J. Chem. Phys. **134**, 144508 (2011).

[16] Y. Shinohara, W. Dmowski, T. Iwashita, D. Ishikawa, A. Q. R. Baron, and T. Egami, Local self-motion of water through the van hove function, Phys. Rev. E **102**, 032604 (2020).

[17] A. Q. R. Baron, High-Resolution inelastic x-ray scattering I: Context, spectrometers, samples, and superconductors, in *Synchrotron Light Sources and Free-Electron Lasers*, edited by E. J. Jaeschke, S. Khan, J. R. Schneider, and J. B. Hastings (Springer, Cham, 2016), pp. 1643–1719.

[18] A. Q. R. Baron, High-resolution inelastic x-ray scattering II: scattering theory, harmonic phonons, and calculations, in *Synchrotron Light Sources and Free-Electron Lasers*, edited by E. Jaeschke, S. Khan, J. R. Schneider, and J. B. Hastings (Springer, Cham, 2016), pp. 1721–1757.

[19] M. B. Stone, J. L. Niedziela, D. L. Abernathy, L. DeBeer-Schmitt, G. Ehlers, O. Garlea, G. E. Granroth, M. Graves-Brook, A. I. Kolesnikov, A. Podlesnyak, and B. Winn, A comparison of four direct geometry time-of-flight spectrometers at the Spallation Neutron Source, Rev. Sci. Instrum. **85**, 045113 (2014).

[20] L. Van Hove, Correlations in space and time and born approximation scattering in systems of interacting particles, Phys. Rev. **95**, 249 (1954).

[21] D. L. Abernathy, M. B. Stone, M. J. Loguillo, M. S. Lucas, O. Delaire, X. Tang, J. Y. Y. Lin, and B. Fultz, Design and operation of the wide angular-range chopper spectrometer ARCS at the spallation neutron source, Rev. Sci. Instrum. **83**, 015114 (2012).

[22] O. Arnold *et al.*, Mantid—data analysis and visualization package for neutron scattering and μ SR experiments, Nucl. Instrum. Methods Phys. Res. A **764**, 156 (2014).

[23] Y. Shinohara, W. Dmowski, T. Iwashita, D. Ishikawa, A. Q. R. Baron, and T. Egami, Local correlated motions in aqueous solution of sodium chloride, Phys. Rev. Mater. **3**, 065604 (2019).

[24] A. Q. R. Baron, Status of the RIKEN quantum nanodynamics beamline (BL43LXU): The next generation for inelastic x-ray scattering, SPring-8 Inf. Newsl. **15**, 14 (2010).

[25] Y. Shinohara, W. Dmowski, T. Iwashita, B. Wu, D. Ishikawa, A. Q. R. Baron, and T. Egami, Viscosity and real-space molecular motion of water: Observation with inelastic x-ray scattering, Phys. Rev. E **98**, 022604 (2018).

[26] V. F. Sears, Neutron scattering lengths and cross sections, Neutron News **3**, 26 (1992).

[27] F. Perakis *et al.*, Coherent x-rays reveal the influence of cage effects on ultrafast water dynamics, Nat. Commun. **9**, 1917 (2018).

[28] R. Mills and K. R. Harris, The effect of isotopic substitution on diffusion in liquids, Chem. Soc. Rev. **5**, 215 (1976).

[29] J. S. Murday and R. M. Cotts, Self-diffusion in liquids: H_2O, D_2O, and Na, J. Chem. Phys. **53**, 4724 (1970).

[30] D. Laage, Reinterpretation of the liquid water quasi-elastic neutron scattering spectra based on a nondiffusive jump reorientation mechanism, J. Phys. Chem. B **113**, 2684 (2009).

[31] R. Yuan, J. A. Napoli, C. Yan, O. Marsalek, T. E. Markland, and M. D. Fayer, Tracking aqueous proton transfer by two-dimensional infrared spectroscopy and ab initio molecular dynamics simulations, ACS Cent. Sci. **5**, 1269 (2019).